Physics Letters B 822 (2021) 136681

Contents lists available at ScienceDirect

Physics Letters B

www.elsevier.com/locate/physletb

Rapidity distributions of $Z = 1$ isotopes and the nuclear symmetry energy from Sn+Sn collisions with radioactive beams at 270 MeV/nucleon

SπRIT Collaboration

M. Kaneko [a,b,*], T. Murakami [a], T. Isobe [b], M. Kurata-Nishimura [b], A. Ono [c], N. Ikeno [d], J. Barney [e,f], G. Cerizza [e], J. Estee [e,f], G. Jhang [e], J.W. Lee [g], W.G. Lynch [e,f], C. Santamaria [e], C.Y. Tsang [e,f], M.B. Tsang [e,f], R. Wang [e], D.S. Ahn [b,h], L. Atar [i,j], T. Aumann [i,j], H. Baba [b], K. Boretzky [j], J. Brzychczyk [l], N. Chiga [b], N. Fukuda [b], I. Gašparić [k], B. Hong [g], A. Horvat [i,j], T. Ichihara [b], K. Ieki [q], N. Inabe [b], Y.J. Kim [p], T. Kobayashi [c], Y. Kondo [o], P. Lasko [m], H.S. Lee [p], Y. Leifels [j], J. Łukasik [m], J. Manfredi [e,f], A.B. McIntosh [r], P. Morfouace [e], T. Nakamura [o], N. Nakatsuka [a,b], S. Nishimura [b], R. Olsen [r], H. Otsu [b], P. Pawłowski [m], K. Pelczar [n], D. Rossi [j], H. Sakurai [b], H. Sato [b], H. Scheit [i], R. Shane [e], Y. Shimizu [b], H. Simon [j], T. Sumikama [b], D. Suzuki [b], H. Suzuki [b], H. Takeda [b], S. Tangwancharoen [e], Y. Togano [q,o], H. Törnqvist [i,j], Z. Xiao [t], S.J. Yennello [r,s], J. Yurkon [e], Y. Zhang [t]

[a] *Department of Physics, Kyoto University, Kyoto 606-8502, Japan*
[b] *RIKEN Nishina Center, Saitama 351-0198, Japan*
[c] *Department of Physics, Tohoku University, Sendai 980-8578, Japan*
[d] *Department of Life and Environmental Agricultural Sciences, Tottori University, Tottori 680-8551, Japan*
[e] *National Superconducting Cyclotron Laboratory, Michigan State University, East Lansing, MI 48824, USA*
[f] *Department of Physics and Astronomy, Michigan State University, East Lansing, MI 48824, USA*
[g] *Department of Physics, Korea University, Seoul 02841, Republic of Korea*
[h] *Korea Basic Science Institute, Daejeon 34133, Republic of Korea*
[i] *Institut für Kernphysik, Technische Universität Darmstadt, D-64289 Darmstadt, Germany*
[j] *GSI Helmholtzzentrum für Schwerionenforschung GmbH, D-64291 Darmstadt, Germany*
[k] *Division of Experimental Physics, Ruđer Bošković Institute, HR-10002 Zagreb, Croatia*
[l] *Faculty of Physics, Astronomy and Applied Computer Science, Jagiellonian University, Pl-30-348 Kraków, Poland*
[m] *Institute of Nuclear Physics, Polish Academy of Sciences, Pl-31-342 Kraków, Poland*
[n] *INFN-Laboratori Nazionali del Gran Sasso, 67100 L'Aquila, Italy*
[o] *Department of Physics, Tokyo Institute of Technology, Tokyo 152-8551 Japan*
[p] *Rare Isotope Science Project, Institute for Basic Science, Daejeon 34047, Republic of Korea*
[q] *Department of Physics, Rikkyo University, Tokyo 171-8501, Japan*
[r] *Cyclotron Institute, Texas A&M University, College Station, TX 77843, USA*
[s] *Department of Chemistry, Texas A&M University, College Station, TX 77843, USA*
[t] *Department of Physics, Tsinghua University, Beijing 100084, PR China*

ARTICLE INFO

Article history:
Received 17 November 2020
Received in revised form 13 September 2021
Accepted 22 September 2021
Available online 27 September 2021
Editor: B. Blank

Keywords:

ABSTRACT

The rapidity distributions of hydrogen isotopes emitted from central collisions of neutron-rich ^{132}Sn+^{124}Sn and neutron-deficient ^{108}Sn+^{112}Sn systems at 270 MeV/nucleon were investigated at RIKEN-RIBF. The data are compared with antisymmetrized molecular dynamics (AMD) calculations and the rapidity distributions can be reproduced after adjusting the in-medium nucleon-nucleon cross sections. The double ratios between the two reaction systems taken for the relative yields of deuteron to proton (d/p) and triton to proton (t/p) are further examined in the midrapidity domain, where the adjustments in the AMD calculations do not affect much on them. The d/p and t/p double ratios at midrapidity agree well with the ratio of the system neutron numbers and its squared value, respectively, and the rapidity

* Corresponding author.
E-mail address: masanori.kaneko@riken.jp (M. Kaneko).

https://doi.org/10.1016/j.physletb.2021.136681

Heavy radioactive isotope collisions
Cluster productions
Nuclear symmetry energy
Antisymmetrized molecular dynamics

dependence of these double ratios is consistent with a picture of partial mixing of colliding nuclei. By comparing with the AMD model which shows a strong symmetry energy dependence of the t/p double ratio, the experimental result in the midrapidity domain favors the calculation with a symmetry-energy slope parameter around $L = 46$ MeV rather than $L = 108$ MeV.

1. Introduction

The density dependence of the symmetry energy term in the nuclear equation of state (EOS) is critically important for elucidating the properties of nuclear systems with large neutron-proton asymmetries [1–3]. Inside neutron stars, where such an environment with a wide range of nuclear densities is realized, the symmetry energy greatly contributes to the pressure and determines the various properties such as the internal composition, the mass–radius relationship, cooling mechanisms, and the tidal deformabilities [4–8]. Although several measurements using nuclear reactions have placed consistent constraints on the symmetry energy below and around the nuclear saturation density, its behavior at high densities is still uncertain [3,9,10]. Energetic heavy-ion collisions (HICs) provide a terrestrial means to study nuclear matter at suprasaturation densities.

In the high-density nuclear matter produced in the central part of HICs of neutron-rich nuclei, the symmetry-energy potential repels neutrons from and attracts protons toward the center of the system. This effect modifies the neutron-proton dynamics during collisions and is expected to appear as changes in the kinematics of free nucleons as well as bound clusters (deuterons, tritons, helions, and so on) [11–13]. To enhance the sensitivity to the symmetry energy, the neutron-to-proton yield ratio and the elliptic flow difference have been proposed as promising probes [14–16]. However, precise determination of the neutron yield and spectrum in HIC experiments is difficult due to the problems of detection efficiency and complex backgrounds. As an alternative observable representing the neutron-proton dynamics, the mirror-nuclei ratio of triton to helion (^{3}H/^{3}He) has also been suggested [12,13,17,18], which requires a better understanding of the mechanism of cluster productions.

The importance of cluster emergence in the nuclear medium has been widely discussed in various fields such as studies of thermodynamic properties in nuclear matter [19,20], core-collapse supernova simulations [10], pasta phases in neutron stars [21], and HICs [22–24]. In particular, in HIC experiments at intermediate energies ($0.1 \sim 1$ GeV/nucleon), it has been reported that the abundance of bound clusters occupies a large part of the total charge of the reaction system [25,26]. This implies a considerable impact of clusters on the reaction dynamics [24]. We focus our discussion here on light clusters ($A \leq 4$), which are more abundant than heavier fragments in the energy domain we are considering. On the theoretical side, transport calculations often use coalescence prescriptions [12,27] to recognize clusters at a certain freeze-out time in the solution of a transport equation, while other transport models explicitly consider cluster correlations in the transport equation so that the correlations may affect the time evolution of HICs [23,28–30]. Recent progress in antisymmetrized molecular dynamics (AMD) [31] incorporating cluster correlations has been moderately successful in reproducing the yields of light charged particles [23]. Moreover, it has also been emphasized that the cluster correlations make a drastic impact on the nucleon dynamics and consequently, e.g., on the charged pion ratio π^-/π^+ [28], which has also been predicted to be sensitive to the density dependence of the symmetry energy [32]. Understanding the cluster production is thus of great importance for extracting a reliable EOS from HICs.

Light charged particles from collisions of stable nuclei have previously been systematically measured for wide ranges of system masses and energies [26]. In this letter, we present the rapidity distributions and spectral ratios of hydrogen isotopes emitted from central collisions of neutron-rich ^{132}Sn+^{124}Sn ($N/Z = 1.56$) and neutron-deficient ^{108}Sn+^{112}Sn ($N/Z = 1.2$) systems at 270 MeV/nucleon, aiming to comprehend the cluster production and its relevance to the symmetry energy determination. These are the first systematic measurements of hydrogen isotopes from HICs using "radioactive isotope beams" in the intermediate-energy domain focusing on the isospin degrees of freedom in HICs. In addition, the use of two reactions with the same total charge of the system allows us to efficiently extract the symmetry-energy effect by constructing the ratio observables, which is expected to reduce the contributions of the Coulomb force. The density dependence of the symmetry energy is discussed using double spectral ratios in the midrapidity domain with a comparison with AMD calculations, which has been refined for the dynamical cluster formations. The measurements of this work are complementary to those dealing with the yields of charged pions and their ratio π^-/π^+ in the same Sn+Sn collisions published by our collaboration [33,34] to probe the symmetry energy at high densities.

Through this systematic measurement of hydrogen isotopes, we hope to gain new insights to understand the light cluster production in HICs. Currently, theoretical interpretations of the experimental data on light clusters are scarce, and transport calculations without dynamical cluster correlations have overestimated the proton yield and underestimated of the light cluster yield by a factor of 2–3 [18,26]. In the present work, we use the AMD model refined for dynamical cluster formations. This allows us to directly compare the calculated results and the experimental data to obtain information on the density dependence of the symmetry energy.

2. Experiment

The experiment was performed at the Radioactive Isotope Beam Factory [35] in RIKEN, Japan. Cocktail beams containing either ^{132}Sn or ^{108}Sn radioactive isotopes were produced by ^{238}U primary beams at 345 MeV/nucleon impinging on a 4-mm-thick Be production target or ^{124}Xe beams at the same kinetic energy impinging on a 0.1-mm-thick Be target, respectively. Isotopes of interest in the cocktail beams were identified event by event with the BigRIPS fragment separator [36,37]. The ^{132}Sn and ^{108}Sn beams were produced with more than 40% purity, 4×10^3 particles/s in average, and 268 MeV/nucleon at the midpoint of the target. Enriched targets of ^{124}Sn (608 mg/cm^2) and ^{112}Sn (561 mg/cm^2) were used for the ^{132}Sn and ^{108}Sn beams, respectively.

Charged particles resulting from collisions were detected by the SAMURAI Pion Reconstruction and Ion-Tracker Time Projection Chamber (Sπ RIT-TPC) [38,39] installed inside the SAMURAI dipole magnet [40] with a magnetic field of 0.5 T. The Sn targets were placed 1.5 centimeters upstream of the TPC sensitive volume. A large geometrical coverage in laboratory polar angles of approximately 0°–80° was realized. Further technical details relevant to the Sπ RIT-TPC and the ancillary trigger arrays can be found in Refs. [41–44], which are summarized in Ref. [39,45].

The accumulated data were analyzed using the Sπ RITROOT software package [46–48], which provides a magnetic rigidity and

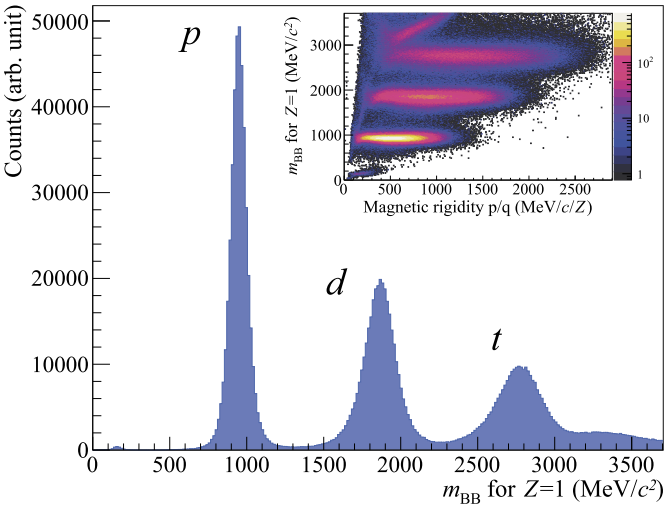

Fig. 1. Mass spectrum around $Z = 1$ particles in central collisions of the ^{132}Sn+^{124}Sn system obtained with the Sπ RIT-TPC and a two-dimensional plot of mass vs. magnetic rigidity magnitude in the right-top panel. The mass m_{BB} was obtained as the solution of the equation in the text.

energy loss per unit length (dE/dx) for each reconstructed track, a reaction vertex reconstruction, and Monte Carlo simulations with the detailed geometry and realistic responses of the Sπ RIT-TPC. To ensure the tracks adopted were reconstructed with high efficiency and high momentum resolution, we restricted the azimuthal angle of the reconstructed tracks to $-30° \leq \phi \leq 20°$ in the analysis. Within this angle, the overall track reconstruction efficiencies of hydrogen isotopes are estimated to be more than 90% using the embedding technique [49]. The momentum resolutions ($\Delta p/p$) are better than 4% in one standard deviation. In this work, we selected central collision events corresponding to $b_0 < 0.15$ in the scaled impact parameter, $b_0 = b/b_{max}$, from the multiplicity of the reconstructed tracks [50]. Here $b_{max} = 1.15\left(A_P^{1/3} + A_T^{1/3}\right)$ fm is based on the sharp nuclear boundary approximation [51] with the mass number of a projectile nucleus A_P and that of a target nucleus A_T.

Fig. 1 presents the mass spectrum for hydrogen isotopes in central events ($b_0 < 0.15$) of ^{132}Sn+^{124}Sn observed in the Sπ RIT-TPC together with the two-dimensional spectrum of mass vs. magnetic rigidity in its inset. The mass (m_{BB}) of a particle was obtained by numerically solving the equation $\langle dE/dx\rangle_{TPC} - (dE/dx)_{BB} = 0$, where $\langle dE/dx\rangle_{TPC}$ denotes dE/dx of the reconstructed tracks and $(dE/dx)_{BB}$ is the empirical Bethe-Bloch function. The parameters of $(dE/dx)_{BB}$ are optimized by the global least χ^2 fit of the $\langle dE/dx\rangle_{TPC}$ vs. magnetic rigidity spectra of hydrogen isotopes with the $Z = 1$ constraint in $(dE/dx)_{BB}$. Typical mass resolutions of hydrogen isotopes were about 15% at FWHM for each. Protons, deuterons, and tritons were identified by gating m_{BB}, and isotope contaminations were estimated from the mass spectrum depending on the magnetic rigidity. A clear separation was achieved for protons with a negligibly small contamination (< 1%). For the triton locus, contaminations mainly come from the ^{3}He contribution, which amounts to about 30% at around 500 MeV/c/Z.

3. Results and discussion

Fig. 2 presents the rapidity distributions (dN/dy_0) of hydrogen isotopes for central collisions of ^{132}Sn+^{124}Sn in the left column and ^{108}Sn+^{112}Sn in the right. Here, the abscissa takes a scaled rapidity $y_0 = y/y_{NN}^{c.m.} - 1$, where y is the rapidity of the detected particle in the laboratory frame and $y_{NN}^{c.m.}$ is the rapidity of the nucleon-nucleon (NN) center of mass in the laboratory frame, i.e.,

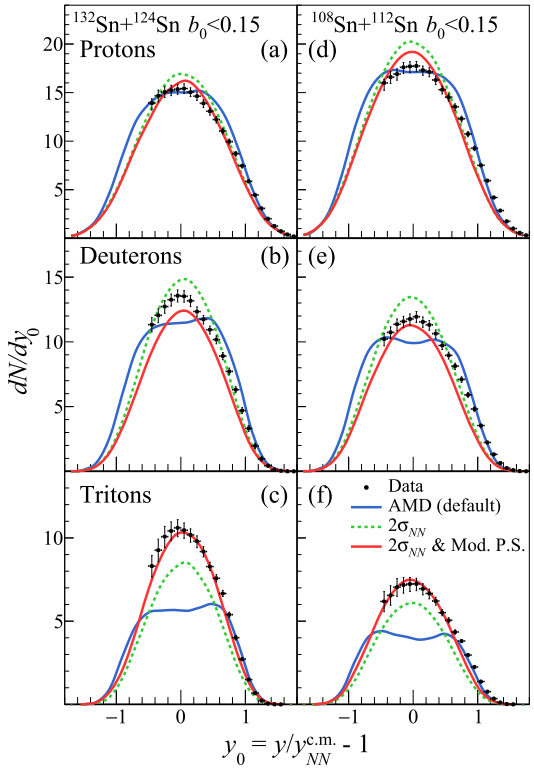

Fig. 2. dN/dy_0 spectra of (a) protons, (b) deuterons and (c) tritons for ^{132}Sn+^{124}Sn of $b_0 < 0.15$ central collisions, and those for ^{108}Sn+^{112}Sn (d)–(f). The black filled circles indicate the experimental data, to which the quadratic sums of the statistical and systematic uncertainties are assigned. AMD predictions with different parameters are shown: the default set of parameters of Ref. [52] (blue dash-dotted lines), the same but for $2 \times \sigma_{NN}$ (green dotted lines, labeled as $2\sigma_{NN}$), and both $2 \times \sigma_{NN}$ and the modified bound phase space for clusters (red solid lines, labeled as $2\sigma_{NN}$ & Mod. P.S.); see the text for details.

$y_{NN}^{c.m.} \approx 0.371$ for both reactions. The statistical uncertainty is approximately 1.5% at midrapidity for all $Z = 1$ isotopes and systems. The systematic uncertainty was estimated by considering the following factors: (1) track-quality assignments, (2) the acceptance associated with the azimuthal angle, (3) gates on m_{BB} for particle identification, (4) isotope contaminations, (5) the presence of a multiplicity filter, (6) the difference observed using full and half data sets, and (7) the effects of the energy deposit in the Sn targets. Variations observed in dN/dy_0 due to the change of the respective factors were around 1–2% for protons and deuterons and 1–4% for tritons. By quadratically summing these values, the systematic uncertainties of the dN/dy_0 spectra were estimated to be about 3%, 3.5%, and 5% for protons, deuterons, and tritons, respectively, for each reaction system. Note that these values are uncertainties averaged over all bins, and the bin-by-bin uncertainties were properly estimated and assigned as shown in Fig. 2.

The yields integrated for the forward rapidity region ($y_0 \geq 0$) of hydrogen isotopes for the two reactions are tabulated in Table 1. The estimated yield of hydrogens ($Z = 1$) in the forward region is about 64–65% of the projectile charge for both reactions while the isotopic fractions differ from each other. The neutron-rich system produced 50% more tritons than the neutron-deficient one, which can be easily understood as reflecting the difference of the neutron number in the system. The agreement of the $Z = 1$ yields for both reactions is not trivial since the two systems have different neutron numbers and it is not clear how the yield depends on this condition. It is worth mentioning that if we double the forward yields of hydrogen isotopes in the central ^{132}Sn+^{124}Sn collisions shown in Table 1, they are consistent with those in a similar sys-

Table 1
Hydrogen isotope yields integrated for the forward rapidity region in the NN center-of-mass frame ($y_0 \geq 0$). Errors include statistical and systematic uncertainties in quadratic sum.

System	Forward p	Forward d	Forward t	Forward $Z=1$
^{132}Sn+^{124}Sn	13.96±0.61	10.64±0.53	7.67±0.33	32.26±0.87
^{108}Sn+^{112}Sn	16.85±0.58	9.81±0.41	5.36±0.22	32.02±0.74

tem of central Xe+CsI collisions at 250 MeV/nucleon reported in Ref. [26].

The data were compared with the AMD calculations from Refs. [23,28,31,52]. In the present work, the Skyrme SLy4 force is employed as an effective interaction. The SLy4 parametrization provides a nuclear symmetry energy of $S_0 = 32.0$ MeV at the saturation density $\rho_0 = 0.16$ fm^{-3} and the symmetry-energy slope parameter $L = 46$ MeV, which we call "asy-soft" in the text. To study another case of a stiff density dependence of the symmetry energy ("asy-stiff"), the density-dependent term in the SLy4 parametrization was modified, as described in Ref. [28]. This asy-stiff parametrization corresponds to $L = 108$ MeV without changing the S_0 value. Cluster correlations are explicitly taken into account in the final states of every two-nucleon collision process, which allows clusters to be formed or disintegrated in the process and then to be propagated according to the equation of motion until the next collision process. The introduction of the cluster correlation mechanism into the heavy-ion collision dynamics is important for resolving the problematic observation that the experimental fragment yield distributions and the stopping quantities are not consistently reproduced by the original AMD calculations without explicit cluster correlations in the dynamical stage [23,52]. The default set of parameters used in this work is the same as the version in Ref. [52], being adjusted to reproduce the results of fragment charge distributions and stopping observables in Xe+CsI reactions at 250 MeV/nucleon [26]. The calculations in the present work were carried out for central collisions with $0 \leq b \leq 1.5$ fm. The maximum density reached in the central compressed region is estimated to be less than twice the saturation density, as indicated by similar transport calculations for central collisions of ^{132}Sn + ^{124}Sn at an incident energy of around 300 MeV/nucleon [28,32].

The calculated dN/dy_0 spectra in the asy-soft case are shown by colored lines in Fig. 2. Because AMD solves the equation of motion in a nonrelativistic scheme, the final momentum of each particle produced in AMD was transferred to the NN center-of-mass frame by the Galilean transformation, and then the rapidity in this frame was calculated. The blue dash-dotted lines indicate the calculated spectra with the default set of parameters of Ref. [52]. The spectra are wider than the data for protons and deuterons, and the integrated yields are moderately similar to the data. For tritons, the yield is well reproduced for $y_0 > 0.8$ while that at midrapidity is underestimated by about 40–50%. This suggests that a mechanism that produces more particles at midrapidity is required. We should therefore carefully investigate whether this mismatch in the nuclear stopping affects the extraction of other physical information such as the density dependence of the symmetry energy. As a test, the in-medium NN cross section (σ_{NN}), reduced from the free NN cross section in the default parametrization of Ref. [52], was increased by a factor of two. As drawn by the green dotted lines in Fig. 2, the shapes of the dN/dy_0 spectra became narrower and comparable to the data. The particle production at midrapidity was enhanced without changing the integrated yields. The shapes of dN/dy_0 do not depend much on the symmetry energy parametrization, including the way they change when σ_{NN} is increased.

As it was found that the total yield of tritons was still about 30% lower than the data, we took a closer look at the production of tritons in the AMD. By examining the time evolution of the triton multiplicity, tritons were found to be recognized sufficiently at relatively early times in the reaction, about 40–50 fm/c after the reaction started, but the number decreased as the reaction time passed. This implies that some clusters are fragile under mean-field propagation and/or under low-energy collisions during the expansion of the system, which could be attributed to the small semi-classical phase space of the bound internal state of light clusters, compared to the quantum phase space. For example, for an $A = 3$ cluster, we can avoid this problem by modifying the phase space so that the bound phase space for the relative coordinate between a two-nucleon pair and another nucleon becomes approximately $(2\pi\hbar)^3$. Such a modification should be effective only when the cluster is almost isolated from the rest of the system. This was technically achieved by introducing a modification factor in the zero-point energy correction term, as in Eq. (C7) of Ref. [53]. The parameters in "term A" row of Table 2 are applied for the correction term in calculations with the asy-soft symmetry energy. The necessary amount of this modification may depend on the original semi-classical phase space determined by the nuclear effective interaction considered, i.e., whether the symmetry energy is asy-soft or asy-stiff in the present study. In the case of the asy-stiff symmetry energy, we use the sum of two terms with parameters of "term A" and "term B" in Table 2 in a similar way to Eq. (C7) of Ref. [53] in order to correct the phase space for $A = 2$ and $A = 3$ clusters. With this correction, the binding energy of deuterons is reasonably reproduced in both the asy-stiff and asy-soft cases. The red solid lines in Fig. 2 are the calculated spectra with $2 \times \sigma_{NN}$ and with this tuning of the bound phase space for clusters. The dN/dy_0 spectra for hydrogen isotopes are now reproduced well.

However, a careful look at Fig. 2 reveals that the peak position of the rapidity distribution dN/dy_0 differs between the experimental data and the calculated results. The peak position is extracted as the mean value μ[1] of a generalized Gaussian probability density function fitted to the dN/dy_0 distribution. In the ^{108}Sn+^{112}Sn system, the peak is located at $\mu \approx -0.021$ in the experimental data and at $\mu \approx -0.020$ in the calculation, which is also close to the rapidity $y_{AA}^{\text{c.m.}} = -0.014$ of the center of mass of the system, if the uncertainty of the fitting $\Delta\mu \sim 0.015$ is taken into account. In the ^{132}Sn+^{124}Sn system, the peak in the calculation is at $\mu \approx 0.032$, consistent with $y_{AA}^{\text{c.m.}} = 0.034$, while the peak in the experimental data is found to be $\mu \approx -0.019$, which deviates significantly from $y_{AA}^{\text{c.m.}}$ to the target side. This anomalous behavior of the peak position in the ^{132}Sn+^{124}Sn system is similarly observed for all hydrogen isotopes, and therefore is not likely related to isospin effects. This calls for a new theoretical interpretation as well as experimental confirmation by systematic studies in the future.

In the following, we mainly use the calculation with $2 \times \sigma_{NN}$ and with the modified bound phase space of clusters, to discuss the density-dependent symmetry energy using the spectral ratio observables. We concentrate on the midrapidity domain where particle emissions from the high-density participant matter are supposed to be dominant. This selection should therefore be appropriate for investigations of the symmetry-energy effect at high densities. In the left panels of Fig. 3, the single spectral ratios constructed for deuterons to protons (d/p) and for tritons to protons (t/p) are shown together with the AMD calculations. Both d/p and t/p have maxima at midrapidity and decrease towards both positive and negative y_0. If the distributions of d/p and t/p are regarded as proportional to the neutron rapidity distribution, i.e.,

[1] As a simplification, a common μ is assumed in the fitting of dN/dy_0 of all hydrogen isotopes in each reaction system. When the peak position is extracted for each of p, d, and t, the values of μ differ from each other by around ±0.01. Later for Fig. 3, we will discuss the partial isospin mixing, which can be qualitatively related to this difference in the peak positions.

Table 2
Parameters used in the modifications for the bound phase space of light clusters. For details on each parameter, see Ref. [53]. "term A" is used for the asy-soft symmetry energy case. The sum of "term A" and "term B" is used in the asy-stiff case.

	ξ	a	$\hat{\xi}$	$\hat{a}$	$\bar{\xi}$	$\bar{a}$	g_0	σ	M	T_0
term A	2.0	0.6	2.0	0.2	1.0	1.2	1.0	0.25	3.0	8.2 MeV
term B							0.52	0.25	2.0	

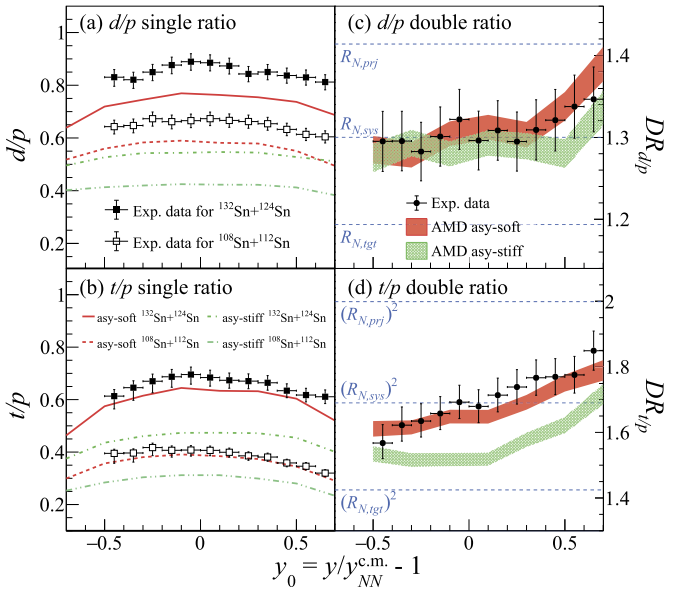

Fig. 3. Single and double spectral ratios of d/p and t/p compared to the AMD calculations with the asy-soft ($L = 46$ MeV) and asy-stiff ($L = 108$ MeV) symmetry energy. The three blue dashed lines in panel (c) indicate the neutron-number ratios of the neutron-rich system to the neutron-deficient system with respect to the projectile nuclei (upper line), target nuclei (lower line), and total system (middle line). In panel (d), the squares of these ratios are shown by the three blue dashed lines; see the text for the details. Note that the vertical-axis ranges of panels (c) and (d) are adjusted so that they are scaled by the neutron-number ratios and the squared ratios, respectively.

as a kind of pseudo-neutron distribution, and the square of it, respectively, then it is naturally understood that they are larger in the neutron-rich ^{132}Sn+^{124}Sn system than in the neutron-deficient ^{108}Sn+^{112}Sn system. The shape of the distribution of pseudo-neutrons seems to be slightly wider than that of protons, as seen in the upper panel of Fig. 2. Whether there is a system difference and thus a symmetry-energy signature in this effect will be discussed in the next paragraph. Here we do not argue much on the absolute values of the theoretical d/p and t/p because these single ratios depend on the fine tuning of the bound phase space for $A = 2$ and $A = 3$ clusters in each case of the symmetry energy. However, we can still reasonably expect that the difference between the ^{132}Sn+^{124}Sn and ^{108}Sn+^{112}Sn systems in each symmetry energy case is not greatly affected by such fine tuning for the clusters. For example, the large system dependence of t/p in the experimental data is not likely to be explained in the asy-stiff case even if the bound phase space for $A = 3$ clusters is further adjusted. In the double ratio observables, the robust part of the information can be extracted.

The right panels of Fig. 3 presents the spectra of the double ratios for d/p and for t/p, which are defined and abbreviated as

$$DR_{d/p} = \frac{d/p\left(^{132}\mathrm{Sn} + ^{124}\mathrm{Sn}\right)}{d/p\left(^{108}\mathrm{Sn} + ^{112}\mathrm{Sn}\right)}, \quad DR_{t/p} = \frac{t/p\left(^{132}\mathrm{Sn} + ^{124}\mathrm{Sn}\right)}{t/p\left(^{108}\mathrm{Sn} + ^{112}\mathrm{Sn}\right)}. \tag{1}$$

These double ratios roughly function as a measure of the neutron populations in the $Z = 1$ particles along rapidity in the neutron-rich system relative to the neutron-deficient system. Most of the systematic uncertainties are canceled in the double ratios. In particular, the uncertainties due to the considerations (1), (3), (4), and (7) above became smaller or almost negligible. The total systematic uncertainties for both $DR_{d/p}$ and $DR_{t/p}$ amounted to about 2.5% at midrapidity.

First we discuss the behavior of the experimental double ratios shown by black symbols in Fig. 3. The value of $DR_{d/p}$ at $y_0 = 0$ agrees with the neutron-number ratio between the two reaction systems denoted by $R_{N,sys} = \left(N_{^{132}\mathrm{Sn}} + N_{^{124}\mathrm{Sn}}\right) / \left(N_{^{108}\mathrm{Sn}} + N_{^{112}\mathrm{Sn}}\right) = (82 + 74) / (58 + 62) = 1.3$. For the t/p double ratio, the value of $DR_{t/p}$ at $y_0 = 0$ agrees with the squared neutron-number ratio $\left(R_{N,sys}\right)^2$, as depicted by the middle blue dashed lines in Fig. 3. Consequently, $\left(DR_{d/p}\right)^2 \simeq DR_{t/p}$ can be interpreted as the light-cluster scaling property also observed in lower-energy HICs [54]. This scaling relation can be explained because the formation probability of deuterons or tritons is proportional to ρ_n or ρ_n^2, respectively, with ρ_n being the neutron density in the region where clusters are made. This neutron density is related to the number of neutrons of the colliding system but can be affected by the symmetry energy and the collision dynamics. However, the observed agreements of $DR_{d/p} \simeq R_{N,sys}$ and $DR_{t/p} \simeq \left(R_{N,sys}\right)^2$ at $y_0 = 0$ indicate that the ratio of ρ_n between the two systems satisfies $R_{\rho_n} \approx R_{N,sys}$ exhibiting a weak effect of the symmetry energy in the midrapidity source. These trends hence can possibly be interpreted as a moderate or weak symmetry energy at high densities, i.e. a soft density dependence of the symmetry energy.

Besides, the $DR_{d/p}$ spectrum is settled down within the range from the neutron-number ratio of the target nuclei ($R_{N,tgt} = N_{^{124}\mathrm{Sn}}/N_{^{112}\mathrm{Sn}}$) to that of the projectile nuclei ($R_{N,prj} = N_{^{132}\mathrm{Sn}}/N_{^{108}\mathrm{Sn}}$), while the $DR_{t/p}$ spectrum is settled down within the range from $\left(R_{N,tgt}\right)^2$ to $\left(R_{N,prj}\right)^2$, as indicated by the blue dashed lines in the right columns of Fig. 3. Though the uncertainties are large, $DR_{d/p}$ at negative and positive y_0 shows almost flat and increasing trends, respectively. $DR_{t/p}$ has an approximately constant positive slope, which is indicative of the difference of the projectile–target asymmetries between the two systems. In the case of ^{132}Sn+^{124}Sn with the neutron-rich projectile, the production of tritons relative to protons is enhanced at forward rapidity compared to ^{108}Sn+^{112}Sn with the neutron-deficient projectile. By introducing a coefficient α, the rapidity dependence of double ratios in the forward region can be parametrized in a similar way. That is, $DR_{d/p} \simeq R_{N,sys} + \alpha_{d/p}\left(R_{N,prj} - R_{N,sys}\right) y_0$ and $DR_{t/p} \simeq \left(R_{N,sys}\right)^2 + \alpha_{t/p}\left((R_{N,prj})^2 - (R_{N,sys})^2\right) y_0$. The least square fit of this parametrization on $DR_{t/p}$ gives $\alpha_{t/p} = 0.69 \pm 0.08$, which is consistent with $\alpha_{d/p} = 0.71 \pm 0.34$ obtained by the fitting on $DR_{d/p}$ only in the forward rapidity domain. If a perfect transparency or a full mixing is achieved in the colliding system, $\alpha = 1$ or 0 would be obtained, respectively. Therefore, the observed behavior can be considered as a partial isospin mixing of the target nucleus and the projectile nucleus.

The red shaded and green cross-stitching areas in the right panels of Fig. 3 are the AMD predictions with $2 \times \sigma_{NN}$ and with the modified bound phase space for clusters based on the pa-

rameters in Table 2. The vertical widths of the calculated spectra represent the statistical errors. The overall trends of the experimental double ratios in the midrapidity domain are reproduced by the calculation, especially by the asy-soft calculation for $DR_{t/p}$. $DR_{t/p}$ is somewhat more sensitive to the symmetry-energy stiffness compared to $DR_{d/p}$. The effects of the density-dependent symmetry energy can appear in the dynamics of HIC, which can be explained as follows. The symmetry-energy potential induces attractive or repulsive forces acting on protons or neutrons, respectively, in a neutron-rich environment. When the two systems are compared, the net effect of the symmetry energy must be larger in the ^{132}Sn+^{124}Sn system than in the ^{108}Sn+^{112}Sn system. In the compression stage of HICs, the high-density symmetry energy contributes to a decrease of the n/p ratio in the central region, and consequently the n/p ratio in the outer surface region is likely to be increased. As shown in Ref. [55], such dynamical effects on the n/p ratios in the central and outer regions are expected to remain in the subsequent expansion stage when clusters start to form, which can be reflected in the emission of particles in the midrapidity domain and higher rapidity domain, respectively. Thus the strong dependence on the stiffness of the symmetry energy seen in the theoretical $DR_{t/p}$ indicates that the main contribution of the triton production likely stems from the central region of the expanding system rather than the outer region. On the other hand, a weaker dependence on the stiffness of the symmetry energy observed for $DR_{d/p}$ may be explained by the fact that deuterons and tritons are produced in slightly different parts of the expanding system, i.e., relatively many deuterons are produced in the outer region of the expanding system as well as in the central region. Then, the symmetry-energy effect of suppressing n/p (and therefore $DR_{d/p}$) in the central region is somewhat canceled by the effect of enhancing n/p (and $DR_{d/p}$) in the outer region.

Finally, to guarantee the robustness of the theoretical calculation with and without the specific modifications provided above, double ratios were also constructed with the two remaining cases of the parameter sets: the default parameter set of Ref. [52] and that with $2 \times \sigma_{NN}$. The differences of double ratios among the calculations using different parameter sets for a specific stiffness of the symmetry energy are consistent within the uncertainties of the experimental data in the midrapidity domain, and thus the conclusions on the symmetry energy do not depend critically on these parameter adjustments.

4. Summary and perspective

In summary, the rapidity distributions of hydrogen isotopes emitted from central collisions of neutron-rich ^{132}Sn+^{124}Sn and those of neutron-deficient ^{108}Sn+^{112}Sn systems at 270 MeV/nucleon were presented. To investigate the stiffness of the symmetry energy, the d/p and t/p double ratios were constructed and compared with AMD calculations under asy-soft and asy-stiff parametrizations. The values of the experimental double ratios at midrapidity were found to be quite similar to the system neutron-number fractions, and the slopes of their rapidity dependences show a partial isospin mixing of two colliding nuclei. The theoretical d/p double ratio did not show strong sensitivity to the stiffness of the symmetry energy, while the t/p double ratio was found to be significantly sensitive. This may suggest some difference between deuterons and tritons in the details of their productions in the expanding system where the neutron and proton densities have been affected by the symmetry energy. In the midrapidity domain, which is supposed to reflect the characteristics of the dense participant matter created by collisions, the experimental t/p double ratio favors the calculation with the asy-soft ($L =$ 46 MeV) symmetry energy rather than the asy-stiff ($L = 108$ MeV) case.

In the rapidity distributions of hydrogen isotopes in the present work, an anomalous behavior was observed in the neutron-rich mass-asymmetric system when the peak position was compared to the rapidity of the center of mass of the system ($y_{AA}^{\mathrm{c.m.}}$). The peak of the experimental dN/dy_0 distribution in the ^{132}Sn+^{124}Sn system deviates from $y_{AA}^{\mathrm{c.m.}}$ to the target side, while the peak in the ^{108}Sn+^{112}Sn system is consistent with $y_{AA}^{\mathrm{c.m.}}$. The AMD calculations predict that the peak should almost agree with $y_{AA}^{\mathrm{c.m.}}$ in both systems. Although the origin of this behavior is not well understood, a slight shift of the rapidity distributions doesn't strongly affect the double ratios in the midrapidity domain and the conclusion on the stiffness of the symmetry energy. Understanding this observation requires further studies.

In the present work, we employed the AMD model, which is an almost unique approach for treating dynamical cluster production in the studied systems. With the modifications to the in-medium nucleon-nucleon cross section, as well as the bound phase spaces for light clusters $A = 2$ and $A = 3$, the experimental dN/dy_0 spectra of hydrogen isotopes are reasonably reproduced by the AMD calculations. However, it is still important to compare the results from different transport codes in order to estimate the theoretical uncertainties, as has been done for the charged pion observables in Ref. [33].

In addition to the $Z = 1$ isotopes presented in this paper, we have measured $Z = 2$ isotopes. The $t/^3$He ratio for the mirror nuclei, which is regarded as a representative probe for the density dependence of the symmetry energy [12,13,17,18], will be investigated in the future to place additional constraints on the EOS of the isospin asymmetric nuclear matter. Although we focused on the stiffness of the symmetry energy here, it would be beneficial to investigate whether the isovector neutron–proton effective mass difference can influence the spectra of $Z = 1$ isotopes [34,56]. The measurement of rapidity distributions is associated with the collision dynamics only in the longitudinal direction, providing a partial probe of the global dynamics. A comprehensive data set on global observables such as collective flow is important to describe the evolution of the collision more completely, which will be available as the data analysis progresses. The description of the rapidity distributions provided in this paper will play an important role for discussing flow observables, since the side flow is expected to be correlated with nuclear stopping [57].

Declaration of competing interest

The authors declare that they have no known competing financial interests or personal relationships that could have appeared to influence the work reported in this paper.

Acknowledgements

This work was supported by the Japanese MEXT KAKENHI (Grant-in-Aid for Scientific Research on Innovative Areas) grant No. 24105004, JSPS KAKENHI Nos. JP17K05432 and JP19K14709, the U.S. Department of Energy under Grant Nos. DE-SC0014530, DE-NA0002923, and DE-FG02-93ER40773, the US National Science Foundation Grant No. PHY-1565546, the Polish National Science Center (NCN), Poland, under contract Nos. UMO-2013/09/B/ST2/04064 and UMO-2013/10/M/ST2/00624, and the National Research Foundation of Korea (NRF) under Grant Nos. 2018R1A5A1025563, 2016K1A3A7A09005578, and 2013M7A1A1075764. I. G. was supported by HIC for FAIR and the Croatian Science Foundation under projects Nos. 1257 and 7194. One of the authors (M. K.) acknowledges the support from the RIKEN Junior Research Associate Program. The computing resource for the data analysis and the theoretical calculations were provided by the HOKUSAI GreatWave

system at RIKEN. The authors also wish to thank the accelerator technical staff at RIBF for the excellent beam supply.

References

[1] P. Danielewicz, R. Lacey, W.G. Lynch, Determination of the equation of state of dense matter, Science 298 (2002) 1592–1596, https://doi.org/10.1126/science.1078070.

[2] M. Baldo, G. Burgio, The nuclear symmetry energy, Prog. Part. Nucl. Phys. 91 (2016) 203–258, https://doi.org/10.1016/j.ppnp.2016.06.006.

[3] C.J. Horowitz, et al., A way forward in the study of the symmetry energy: experiment, theory, and observation, J. Phys. G 41 (2014) 093001, https://doi.org/10.1088/0954-3899/41/9/093001.

[4] J.M. Lattimer, M. Prakash, Neutron star observations: prognosis for equation of state constraints, Phys. Rep. 442 (2007) 109–165, https://doi.org/10.1016/j.physrep.2007.02.003.

[5] J.M. Lattimer, M. Prakash, The equation of state of hot, dense matter and neutron stars, Phys. Rep. 621 (2016) 127–164, https://doi.org/10.1016/j.physrep.2015.12.005.

[6] B.P. Abbott, et al., GW170817: observation of gravitational waves from a binary neutron star inspiral, Phys. Rev. Lett. 119 (2017) 161101, https://doi.org/10.1103/PhysRevLett.119.161101.

[7] F.J. Fattoyev, W.G. Newton, B.-A. Li, Probing the high-density behavior of symmetry energy with gravitational waves, Eur. Phys. J. A 50 (2014) 45, https://doi.org/10.1140/epja/i2014-14045-6.

[8] B.-A. Li, et al., Towards understanding astrophysical effects of nuclear symmetry energy, Eur. Phys. J. A 55 (2019) 117, https://doi.org/10.1140/epja/i2019-12780-8.

[9] M.B. Tsang, et al., Constraints on the symmetry energy and neutron skins from experiments and theory, Phys. Rev. C 86 (2012) 015803, https://doi.org/10.1103/PhysRevC.86.015803.

[10] M. Oertel, et al., Equations of state for supernovae and compact stars, Rev. Mod. Phys. 89 (2017) 015007, https://doi.org/10.1103/RevModPhys.89.015007.

[11] L.-W. Chen, et al., Isospin effects on two-nucleon correlation functions in heavy-ion collisions at intermediate energies, Phys. Rev. C 68 (2003) 014605, https://doi.org/10.1103/PhysRevC.68.014605.

[12] L.-W. Chen, C. Ko, B.-A. Li, Light cluster production in intermediate energy heavy-ion collisions induced by neutron-rich nuclei, Nucl. Phys. A 729 (2003) 809–834, https://doi.org/10.1016/j.nuclphysa.2003.09.010.

[13] L.-W. Chen, C.M. Ko, B.-A. Li, Effects of momentum-dependent nuclear potential on two-nucleon correlation functions and light cluster production in intermediate energy heavy-ion collisions, Phys. Rev. C 69 (2004) 054606, https://doi.org/10.1103/PhysRevC.69.054606.

[14] B.-A. Li, et al., Double neutron/proton ratio of nucleon emissions in isotopic reaction systems as a robust probe of nuclear symmetry energy, Phys. Lett. B 634 (2006) 378–382, https://doi.org/10.1016/j.physletb.2006.02.003.

[15] S. Kumar, et al., Sensitivity of neutron to proton ratio toward the high density behavior of the symmetry energy in heavy-ion collisions, Phys. Rev. C 85 (2012) 024620, https://doi.org/10.1103/PhysRevC.85.024620.

[16] M. Cozma, Neutron–proton elliptic flow difference as a probe for the high density dependence of the symmetry energy, Phys. Lett. B 700 (2011) 139–144, https://doi.org/10.1016/j.physletb.2011.05.002.

[17] G.-C. Yong, et al., Triton-^{3}He relative and differential flows as probes of the nuclear symmetry energy at supra-saturation densities, Phys. Rev. C 80 (2009) 044608, https://doi.org/10.1103/PhysRevC.80.044608.

[18] Y. Wang, et al., ^{3}H/^{3}He ratio as a probe of the nuclear symmetry energy at sub-saturation densities, Eur. Phys. J. A 51 (2015) 37, https://doi.org/10.1140/epja/i2015-15037-8.

[19] S. Typel, et al., Composition and thermodynamics of nuclear matter with light clusters, Phys. Rev. C 81 (2010) 015803, https://doi.org/10.1103/PhysRevC.81.015803.

[20] G. Röpke, Nuclear matter equation of state including two-, three-, and four-nucleon correlations, Phys. Rev. C 92 (2015) 054001, https://doi.org/10.1103/PhysRevC.92.054001.

[21] S.S. Avancini, et al., Light clusters and pasta phases in warm and dense nuclear matter, Phys. Rev. C 95 (2017) 045804, https://doi.org/10.1103/PhysRevC.95.045804.

[22] L. Csernai, J.I. Kapusta, Entropy and cluster production in nuclear collisions, Phys. Rep. 131 (1986) 223–318, https://doi.org/10.1016/0370-1573(86)90031-1.

[23] A. Ono, Cluster correlations in multifragmentation, J. Phys. Conf. Ser. 420 (2013) 012103, https://doi.org/10.1088/1742-6596/420/1/012103.

[24] A. Ono, Dynamics of clusters and fragments in heavy-ion collisions, Prog. Part. Nucl. Phys. 105 (2019) 139–179, https://doi.org/10.1016/j.ppnp.2018.11.001.

[25] S. Hudan, et al., Characteristics of the fragments produced in central collisions of ^{129}Xe+^{nat}Sn from 32A to 50 A MeV, Phys. Rev. C 67 (2003) 064613, https://doi.org/10.1103/PhysRevC.67.064613.

[26] W. Reisdorf, et al., Systematics of central heavy ion collisions in the 1A GeV regime, Nucl. Phys. A 848 (2010) 366–427, https://doi.org/10.1016/j.nuclphysa.2010.09.008.

[27] S. Sood, et al., Cluster formation and phase transition in nuclear disassembly using a variety of clusterization algorithms, Phys. Rev. C 99 (2019) 054612, https://doi.org/10.1103/PhysRevC.99.054612.

[28] N. Ikeno, et al., Probing neutron-proton dynamics by pions, Phys. Rev. C 93 (2016) 044612, https://doi.org/10.1103/PhysRevC.93.044612, Erratum: Phys. Rev. C 97 (2018), 066902(E).

[29] P. Danielewicz, G. Bertsch, Production of deuterons and pions in a transport model of energetic heavy-ion reactions, Nucl. Phys. A 533 (1991) 712–748, https://doi.org/10.1016/0375-9474(91)90541-D.

[30] P. Danielewicz, Q. Pan, Blast of light fragments from central heavy-ion collisions, Phys. Rev. C 46 (1992) 2002–2011, https://doi.org/10.1103/PhysRevC.46.2002.

[31] A. Ono, et al., Antisymmetrized version of molecular dynamics with two-nucleon collisions and its application to heavy ion reactions, Prog. Theor. Phys. 87 (1992) 1185–1206, https://doi.org/10.1143/ptp/87.5.1185.

[32] B.-A. Li, High density behaviour of nuclear symmetry energy and high energy heavy-ion collisions, Nucl. Phys. A 708 (2002) 365–390, https://doi.org/10.1016/S0375-9474(02)01018-7.

[33] G. Jhang, et al., Symmetry energy investigation with pion production from Sn+Sn systems, Phys. Lett. B 813 (2021) 136016, https://doi.org/10.1016/j.physletb.2020.136016.

[34] J. Estee, et al., Probing the symmetry energy with the spectral pion ratio, Phys. Rev. Lett. 126 (2021) 162701, https://doi.org/10.1103/PhysRevLett.126.162701.

[35] Y. Yano, The RIKEN RI beam factory project: a status report, Nucl. Instrum. Methods Phys. Res., Sect. B 261 (2007) 1009–1013, https://doi.org/10.1016/j.nimb.2007.04.174.

[36] T. Kubo, et al., BigRIPS separator and ZeroDegree spectrometer at RIKEN RI Beam Factory, Prog. Theor. Exp. Phys. 2012 (2012) 03C003, https://doi.org/10.1093/ptep/pts064.

[37] N. Fukuda, et al., Identification and separation of radioactive isotope beams by the BigRIPS separator at the RIKEN RI Beam Factory, Nucl. Instrum. Methods Phys. Res., Sect. B 317 (2013) 323–332, https://doi.org/10.1016/j.nimb.2013.08.048.

[38] R. Shane, et al., Sπ RIT: a time-projection chamber for symmetry-energy studies, Nucl. Instrum. Methods Phys. Res., Sect. A 784 (2015) 513–517, https://doi.org/10.1016/j.nima.2015.01.026.

[39] J. Barney, et al., The sπ RIT time projection chamber, arXiv:2005.10806.

[40] H. Sato, et al., Superconducting dipole magnet for SAMURAI spectrometer, IEEE Trans. Appl. Supercond. 23 (2013) 4500308, https://doi.org/10.1109/TASC.2012.2237225.

[41] T. Isobe, et al., Application of the Generic Electronics for Time Projection Chamber (GET) readout system for heavy Radioactive isotope collision experiments, Nucl. Instrum. Methods Phys. Res., Sect. A 899 (2018) 43–48, https://doi.org/10.1016/j.nima.2018.05.022.

[42] S. Tangwancharoen, et al., A gating grid driver for time projection chambers, Nucl. Instrum. Methods Phys. Res., Sect. A 853 (2017) 44–52, https://doi.org/10.1016/j.nima.2017.02.001.

[43] M. Kaneko, et al., Kyoto Multiplicity Array for the Sπ RIT experiment, RIKEN Accel. Prog. Rep. 50 (2017) 172.

[44] P. Lasko, et al., KATANA – a charge-sensitive triggering system for the Sπ RIT experiment, Nucl. Instrum. Methods Phys. Res., Sect. A 856 (2017) 92–98, https://doi.org/10.1016/j.nima.2017.03.006.

[45] J.E. Barney, Charged pion emission from ^{112}Sn+^{124}Sn and ^{124}Sn+^{112}Sn reactions with the Sπ RIT time projection chamber, Ph.D. thesis, Michigan State University, 2019.

[46] J.W. Lee, et al., Charged particle track reconstruction with Sπ RIT time projection chamber, Nucl. Instrum. Methods Phys. Res., Sect. A 965 (2020) 163840, https://doi.org/10.1016/j.nima.2020.163840.

[47] J. Estee, et al., Extending the dynamic range of electronics in a Time Projection Chamber, Nucl. Instrum. Methods Phys. Res., Sect. A 944 (2019) 162509, https://doi.org/10.1016/j.nima.2019.162509.

[48] C.Y. Tsang, et al., Space charge effects in the Sπ RIT time projection chamber, Nucl. Instrum. Methods Phys. Res., Sect. A 959 (2020) 163477, https://doi.org/10.1016/j.nima.2020.163477.

[49] M. Anderson, et al., The STAR time projection chamber: a unique tool for studying high multiplicity events at RHIC, Nucl. Instrum. Methods Phys. Res., Sect. A 499 (2003) 659–678, https://doi.org/10.1016/S0168-9002(02)01964-2.

[50] C. Cavata, et al., Determination of the impact parameter in relativistic nucleus-nucleus collisions, Phys. Rev. C 42 (1990) 1760–1763, https://doi.org/10.1103/PhysRevC.42.1760.

[51] W.D. Myers, Geometric properties of leptodermous distributions with applications to nuclei, Nucl. Phys. A 204 (1973) 465–484, https://doi.org/10.1016/0375-9474(73)90388-6.

[52] A. Ono, Impacts of cluster correlations on heavy-ion collision dynamics, in: Proceedings of 13th International Conference on Nucleus-Nucleus Collisions, Journal of the Physical Society of Japan, Saitama, Japan, 2020.

[53] A. Ono, H. Horiuchi, T. Maruyama, Nucleon flow and fragment flow in heavy ion reactions, Phys. Rev. C 48 (1993) 2946–2955, https://doi.org/10.1103/PhysRevC.48.2946.

[54] Z. Chajecki, et al., Scaling properties of light-cluster production, arXiv:1402.5216 [nucl-ex].

[55] A. Ono, Cluster production within transport theory, EPJ Web Conf. 117 (2016) 07003, https://doi.org/10.1051/epjconf/201611707003.
[56] J. Su, et al., Effects of symmetry energy and effective k-mass splitting on central ^{96}Ru(^{96}Zr)+^{96}Zr(^{96}Ru) collisions at 50 to 400 MeV/nucleon, Phys. Rev. C 96 (2017) 024601, https://doi.org/10.1103/PhysRevC.96.024601.
[57] W. Reisdorf, et al., Nuclear stopping from 0.09A to 1.93A GeV and its correlation to flow, Phys. Rev. Lett. 92 (2004) 232301, https://doi.org/10.1103/PhysRevLett.92.232301.